Silicon nanocrystals functionalized with photoactive units for dual-potential electrochemiluminescence

Silicon Nanocrystals functionalized with photoactive units for dual-potential electrochemiluminescence

Giacomo Morselli, Francesco Romano, Giovanni Valenti, Francesco Paolucci, Paola Ceroni**

AUTHOR ADDRESS

Department of Chemistry "Giacomo Ciamician", University of Bologna, 40126, Bologna, Italy

ABSTRACT

Silicon nanocrystals (SiNCs) have attracted attention due to their unique properties that render them particularly suitable for a high variety of applications, such as ECL sensors. However, the electrochemiluminescence of SiNCs has not been investigated in depth so far and the research has been focused on conventional quantum dots composed of toxic or rare materials. Here, we investigate the ECL properties of heterosupramolecular systems based on organic chromophores (diphenylanthracene, DPA) linked onto the SiNC's surface. The optical properties of the nanocrystal are affected by the presence of the chromophores; their ECL behaviors are independent each other and that generates hybrid systems characterized by a dual-potential electrochemiluminescence. These nanoparticles can be used as single-systems with tunable dual-potential emissions: the ECL signals can be varied with the type of the attached chromophore.

INTRODUCTION

Electrochemiluminescence (ECL) is a chemiluminescence where the excited state generation is induced by an electrochemical stimulus.[1,2] ECL is a leading transduction techniques in immunosensors extensively studied for *in vitro* diagnosis and light-emitting devices.[3–5]

Thanks to the absence of excitation light, ECL owns unique properties such as very low background and high sensitivity. In particular, ECL has been a great success in the biosensor fields, thanks to the unique signal-to-noise ratio also in real and very complex matrixes.

The combination between ECL and nanomaterials is one of the most promising approaches in the biosensing field to ameliorate the amplification signal. Nanomaterials has been largely used to increase (i) the efficiency of electron transfer process[6] and (ii) the number of ECL dyes or the ECL efficiency for recognition event.[7,8] Concerning the latter cases the most applied nanomaterials are quantum dots (QDs),[9,10] carbon dots,[11,12] polymer dots[13] or dye-doped nanoparticles.[14,15] Cao *et al.* recently showed the advantages of core/shell cadmium-based quantum dots over conventional emitters, including an enhancement in ECL efficiency and the size-dependent emission.[16] Moreover,

the sensitivity of ECL-based sensing techniques can be further ameliorated coupling quantum and carbon dots with species which are electrochemiluminescent at different potentials, such as luminol-gold nanoparticles for the detection of telomerase, malachite green and chloramphenicol.[17,18] These "dual-potential" systems allow a ratiometric measurement by recording the ECL intensities at two different potentials and calculating their ratio.[19,20]

Amid quantum dots, silicon nanocrystals (SiNCs) are a valid alternative for numerous purposes, due to the abundance of silicon and its non-toxicity.[21] SiNCs are ideal nanomaterials for ECL applications thanks to their high photoluminescence quantum yield, which increases the chemiluminescence intensity, a high stability and a long-lived emission in red/near-infrared spectral range, which is tunable accordingly with their size.[21] Despite their qualities, only few studies focused on the ECL behavior of SiNCs. Bard and co-workers pioneering reported the generation of ECL from blue-photoluminescent SiNCs, whose signal was, contrary to photoluminescence, size-independent.[22] Afterwards, Dong *et al.*[23,24] investigated the ECL biosensing applications of water-suspendable SiNCs, which were, however, synthesized with a severely criticized approach[25,26] and therefore it is not possible to correlate the ECL signal to silicon effectively. Porous silicon ECL was studied more extensively, but only few ECL cycles were stable and reproducible because of an irreversible oxidation.[27–32]

An interesting characteristic of SiNCs is the possibility to link through covalent bonds different molecules, e.g. chromophores that can ameliorate the optical properties of the quantum dot.[33–37]

In this context our group recently reported the synthesis of silicon nanocrystals functionalized with organic molecules such as 9,10-diphenylanthracene (DPA).[36] Here, we demonstrate that this functionalization generates a heterosupramolecular system characterized by a dual-potential electrochemiluminescence due to the attached chromophore and the silicon nanoparticle. Although there are several examples of quantum dots which display various ECL at different potentials, none of them are characterized by a single-system, nor act at the same electrode (i.e. reductive potential).[17–

[20,38–41] Furthermore, this is the first work that studies the electrochemical behavior of chromophore-functionalized silicon nanocrystals.

EXPERIMENTAL SECTION

All reagents were purchased from Sigma-Aldrich and used without further purification if not stated otherwise. Dry toluene was obtained via distillation over calcium chloride under nitrogen atmosphere. N,N,N',N'-tetramethylethylenediamine was refluxed over fresh KOH and distilled under nitrogen.

1. Synthesis of silicon nanocrystals

The synthesis of DPA-functionalized SiNCs has already been discussed in a previous paper.[36] However, the procedures are here reported.

Preparation of oxide-embedded silicon nanocrystal. Hydrogen silsesquioxane (HSQ) was prepared from $HSiCl_3$ as starting material following a reported procedure,[42] dried under vacuum and transferred into a tube furnace. After purging with reducing gas (95% N_2, 5% H_2), the tube furnace was heated to 1100°C or 1025°C at a rate of 18°C/min and then held at that temperature for an hour. The resulting solid was cooled to room temperature, manually and mechanically reduced into brown powder (that is $Si@SiO_2$, i.e. SiNCs embedded in a silica matrix) and stored in a glass vial. The sizes of the nanoparticles obtained by this process were determined by the temperature of annealing of HSQ, as reported in literature.[43] At 1100°C, SiNCs with a diameter of about 4 nm were obtained, while at 1025°C, nanoparticles with about 3-nm diameter were formed.

Synthesis of hydride-terminated silicon nanocrystals. Hydride-terminated silicon nanocrystals were liberated from the silica matrix by HF etching (***caution!*** *HF is very dangerous and must be handled very carefully!)*: 300 mg of oxide-embedded silicon nanocrystals were dispersed in a mixture composed of 3 mL of ethanol, 3 mL of bi-distilled water and 3 mL of a 49% solution of aqueous HF. The mixture was stirred for 90 minutes under ambient light at room temperature. The nanocrystals

were extracted with toluene (3x10 mL) and then centrifuged three times in toluene (8000 rpm for 5 minutes). The nanocrystals were then transferred in a dry box.

Passivation with chloro(dimethyl)vinylsilane or dodecene (Si-DDE). The nanocrystals were dispersed in 4 mL of dry toluene and split in two portions. Two milligrams of 4-decyldiazobenzene tetrafluoroborate (about 6 μmol) were added in each one. Afterwards, in one mixture, chloro(dimethyl)vinylsilane (1.5 mmol) was introduced to obtain chlorosilane-passivated silicon nanocrystals. In the other one, 1-dodecene (1.5 mmol) was dropped, to passivate the nanocrystals with an alkyl chain. Both mixtures were stirred overnight at room temperature. The mixture of chlorosilane-passivated SiNCs was then filtered, concentrated at reduced pressure, transferred again in the dry-box, diluted with 2 mL of dry toluene and conserved for a further functionalization. The suspension of dodecyl-passivated nanocrystals was precipitated by adding methanol and centrifuged three times washing with methanol. The precipitate was dissolved in dichloromethane (DCM) or tetrahydrofuran (THF), obtaining **Si_{3nm}-DDE** and **Si_{4nm}-DDE** indicating dodecyl-passivated SiNCs with an average diameter of 3 or 4 nm.

Functionalization of silicon nanocrystals with diphenylanthracene (Si-DPA). 9-phenyl-10-(4-((prop-2-yn-1-yloxy)methyl)phenyl)anthracene (0.3 mmol) was introduced in a flask containing 0.45 mmol of N,N,N',N'-tetramethylethylenediamine (TMEDA) and 3 mL of dry toluene. At -78°C, n-butyllithium (nBuLi 0.3 mmol) 2.5 M in hexanes was added dropwise under inert atmosphere (***caution!*** *n-butyllithium is pyrophoric!*). The mixture was stirred for 45 minutes at -78°C and 15 minutes at room temperature. Again at -78°C, a suspension of chlorosilane-passivated silicon nanocrystals in toluene was slowly added to the reaction mixture. One hour later, the reaction mixture was stirred for an hour at room temperature. Later, it was heated to 40°C, and stirred for another hour. At -78°C a second amount of nBuLi (0.15 mmol) was added before letting the mixture stir overnight at room temperature. The reaction was quenched with several mL of a 1 M solution of HCl in MeOH. The precipitate was washed 3 times with methanol, centrifuging (8000 rpm, 5 minutes) and then

dispersed in chloroform. A size exclusion chromatography over BioBeadsTM S-X1 Support (200-400 mesh) was performed to isolate a brown limpid suspension, yielding the **Si-DPA** samples (**Si_{3nm}-DPA** or **Si_{4nm}-DPA** for, respectively, diphenylanthracene-functionalized SiNCs with an average diameter of 3 or 4 nm). ^{1}H-NMR ($CDCl_3$, 400 MHz) was used to assess the occurring of the functionalization (Figure S1). The sample was then dispersed in DCM or THF.

2. Photophysical measurements

Photophysical measurements were carried out in air-equilibrated tetrahydrofuran at 298 K. UV-visible absorbance spectra were recorded with a Perkin Elmer λ650 spectrophotometer, using quartz cells with 1.0 cm path length. Emission spectra were obtained with either a Perkin Elmer LS-50 spectrofluorometer, equipped with a Hamamatsu R928 phototube, or an Edinburgh FLS920 spectrofluorometer equipped with a Ge-detector for emission in the NIR spectral region. Correction of the emission spectra for detector sensitivity in the 550-1000 nm spectral region was performed by a calibrated lamp.[44,45] Emission quantum yields were measured following the method of Demas and Crosby[46] (standard used: $[Ru(bpy)_3]^{2+}$ in air-equilibrated aqueous solution $\Phi = 0.0407$).

Photophysical characterization was also used to assess the size of the nanoparticles obtained, due to the univocal correlation between emissive properties and the size of the nanoparticles, as assessed by Yu *et al*.[47] 4-nm sized SiNCs passivated with a dodecyl chain (**Si_{4nm}-DDE**) have a maximum emission at about 780 nm, while 3-nm sized ones (**Si_{3nm}-DDE**) emit at around 680 nm (Figure 2). Chromophore-functionalized SiNCs are characterized by a red-shifted emission which has been noticed also for other SiNCs based antennae and that is not related to a different size of the samples.[33]

3. ECL apparatus and ECL measurements

ECL and electrochemical measurements were carried out with an AUTOLAB electrochemical station (Ecochemie, Mod. PGSTAT 30). The ECL signal generated by performing the potential step program was measured with a photomultiplier tube (PMT, Hamamatsu P980) placed, at a constant distance in front of the working electrode, under the cell and inside a homemade dark box. A voltage in the range 550−750 V was supplied to the PMT. The light/current/voltage curves were recorded by collecting

the preamplified PMT output signal (by an ultralow noise Acton research model 181) with the second input channel of the ADC module of the AUTOLAB instrument.

ECL spectra have been recorded by inserting the same PMT in a dual-exit monochromator (ACTON RESEARCH model Spectra Pro2300i) and collecting the signal as described at a fixed voltage vs Ag QRE.

Photocurrent detected at PMT was accumulated for 1-3 s, depending on the emission intensity, for each monochromator wavelength step (usually 1 or 2 nm).

For ECL measurements, a cylindrical three electrodes electrochemiluminescence cell with PTFE stopcock and a Schlenk-like connection to the vacuum-inert gas line was used. As working electrode, platinum was chosen, as quasi-reference electrode, silver, and as counter electrode, a spiral-shaped platinum wire.

For the measurements in dichloromethane (DCM), a batch of dodecyl-passivated or DPA-functionalized SiNCs derived from the etching of 100 mg of $Si@SiO_2$ powder in 3 mL of DCM (about 1 μM) was introduced in the cell. 500 mg of $TBAPF_6$ (0.4 M) and 50 μL of tripropylamine (TrPA) (0.08 M) were subsequently added. The suspension was degassed with Ar. For the measurements in tetrahydrofuran (THF), the same procedure was performed, but 300 mg of $TBAPF_6$ (0.25 M) and 10 mg of benzoyl peroxide, BPO, (10 mM) were added instead in 3 mL of solvent. In each solution, two or three records were made to check the temporal stability of the system investigated.

RESULTS AND DISCUSSION

DPA-functionalized and dodecyl-passivated SiNCs with a diameter of 3 or 4 nm (**Si_{3nm}-DPA**, **Si_{4nm}-DPA**, **Si_{3nm}-DDE** or **Si_{4nm}-DPA**) were obtained by a functionalization of hydride-terminated silicon nanocrystals, obtained by disproportionation of hydrogen silsesquioxane (HSQ, $[HSiO_{3/2}]_n$) followed by etching process.[42,48,49] The surface functionalization[36] with the organic chromophore consisted in a two-step procedure: (i) hydrosilylation with chloro(dimethyl)vinylsilane promoted by

diazonium salts (4-decylbenzene diazonium tetrafluoroborate),[50] yielding chlorosilane-passivated SiNCs, (ii) post-functionalization by nucleophilic reagents: in the present case, an acetylide derivative of diphenylanthracene formed *in situ* with nBuLi, yielding the **Si-DPA** samples (Figure 1a). As control sample, alkyl-capped SiNCs (**Si-DDE**, Figure 1b) were prepared by direct hydrosilylation of hydrogen-terminated silicon nanocrystals in presence of 1-dodecene and initiated with diazonium salts (see Experimental Section for further details). For simplicity purposes, we will adress to 3-nm sized dodecyl-passivated and diphenylanthracene-functionalized SiNCs as **Si_{3nm}-DDE** and **Si_{3nm}-DPA**. In the same way, **Si_{4nm}-DDE** and **Si_{4nm}-DPA** are referred to 4-nm sized SiNCs.

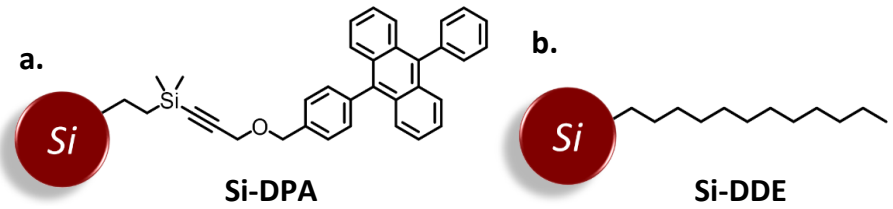

Figure 1. *Schematic representation of (a) 9,10-Diphenylanthracene-functionalized silicon nanocrystals (**Si-DPA**) and (b) dodecyl-passivated silicon nanocrystals (**Si-DDE**). For simplicity purposes, only one ligand per nanocrystal has been drawn.*

The absorption spectra of diphenylanthracene-functionalized SiNCs (solid blue lines in Figure 2) show the contribution of DPA (the absorption spectrum of the ligand alone is given in Figure 2, black line) with sharp peaks in the interval 350-410 nm and a tail due to silicon nanocrystals extending up to 550 nm. From the absorption spectra we can evaluate that 80 DPA units are linked per **Si_{4nm}-DPA** and 35 per **Si_{3nm}-DPA**, as an average (further details can be found in the Supporting Information). This results in an enhancement in the absorbance between 350 and 410 nm. As opposed to what happens with an equimolar mixture of free DPA and silicon nanocrystals, the emission of the organic chromophore, following its direct excitation, is quenched. In particular, an energy transfer to the silicon core occurs with an efficiency of 70%,[36] followed by a sensitized emission of the inner silicon nanoparticle at 800 nm (solid red lines in Figure 2). This system acts as a light-harvesting antenna characterized by a brightness superior to the alkyl-passivated silicon nanocrystals' one (exciting at

373 nm, DPA functionalization led to a nearly 150% brightness enhancement in THF for **$Si_{4\ nm}$-DPA**, as discussed in the Supplementary Information).

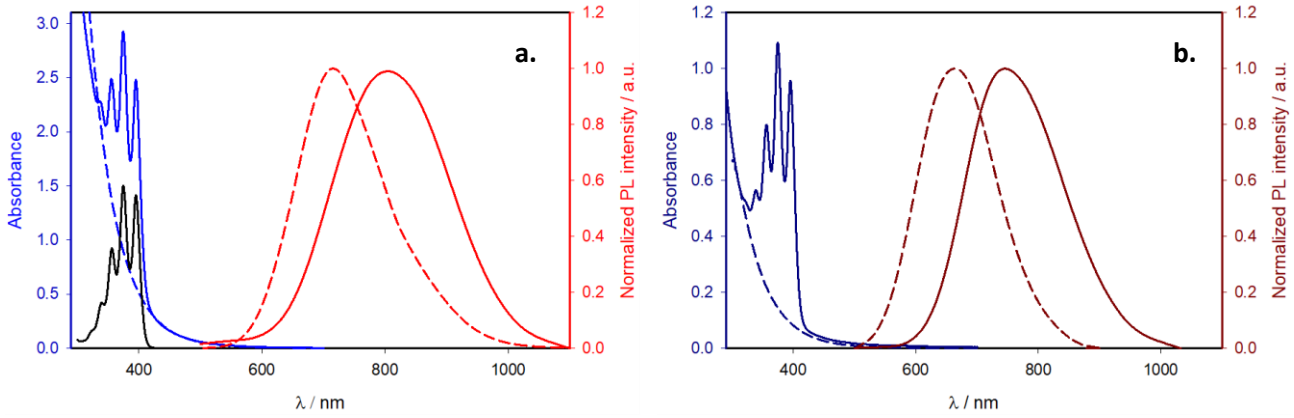

Figure 2. *Absorption (blue lines) and normalized photoluminescence spectra (red lines, excitation at 400 nm) of THF suspension of (a) 4-nm and (b) 3-nm sized DPA-functionalized SiNCs (solid lines) and dodecyl-passivated SiNCs (dashed lines). For comparison purposes, the absorption spectrum of DPA (black line) has been included in panel a.*

The first measurements of electrochemiluminescence were performed in dichloromethane (DCM), using tetrabutylammonium hexafluorophosphate ($TBAPF_6$) as electrolyte and tripropylamine (TrPA) as coreactant. TrPA was chosen because it is known to act as coreactant for the ECL of porous silicon at positive potentials.[27] However, the generation of the excited state of DPA did not occur and a unique ECL due to the silicon nanocrystal was visible for each system (Figure S3). Moreover, after the first cycle, it was possible to notice an aggregation of the nanoparticles, suggesting that either positive potentials or TrPA damage SiNCs.

Therefore, the ECL measurements for dodecyl and DPA-functionalized SiNCs were replicated in different experimental conditions. Firstly, a different coreactant, benzoyl peroxide (BPO), was chosen instead of TrPA. This reagent is known to act as ECL coreactant with a so called "reductive-oxidation" mechanism with aromatic species.[51] At cathodic potentials, BPO is irreversibly reduced and it decomposes in a strong oxidizing species (benzoyloxy radical, PhCOO·), which is able to react

with aromatic compounds reduced at the working electrode, yielding their corresponding excited state.

Moreover, tetrahydrofuran (THF) was chosen as solvent as the photoluminescence emission quantum yield of silicon nanocrystals are high (e.g., 25% and 11% for **Si_{4nm}-DDE** and **Si_{4nm}-DPA**, respectively), it is possible to introduce a lower amount of electrolyte and it is known to well dissolve every components of the mixture.

Cyclic voltammetries (from OCV to -2.5 V vs Ag QRE and back to 0 V) were performed for equimolar suspensions of nanoparticles (Figures S5). Due to the high concentration of BPO with respect to silicon nanoparticles and DPA only BPO reduction is visible (peak potential at -1.3 V, in accordance with the data found in literature[51]). The corresponding ECL signals are reported in Figure 3.

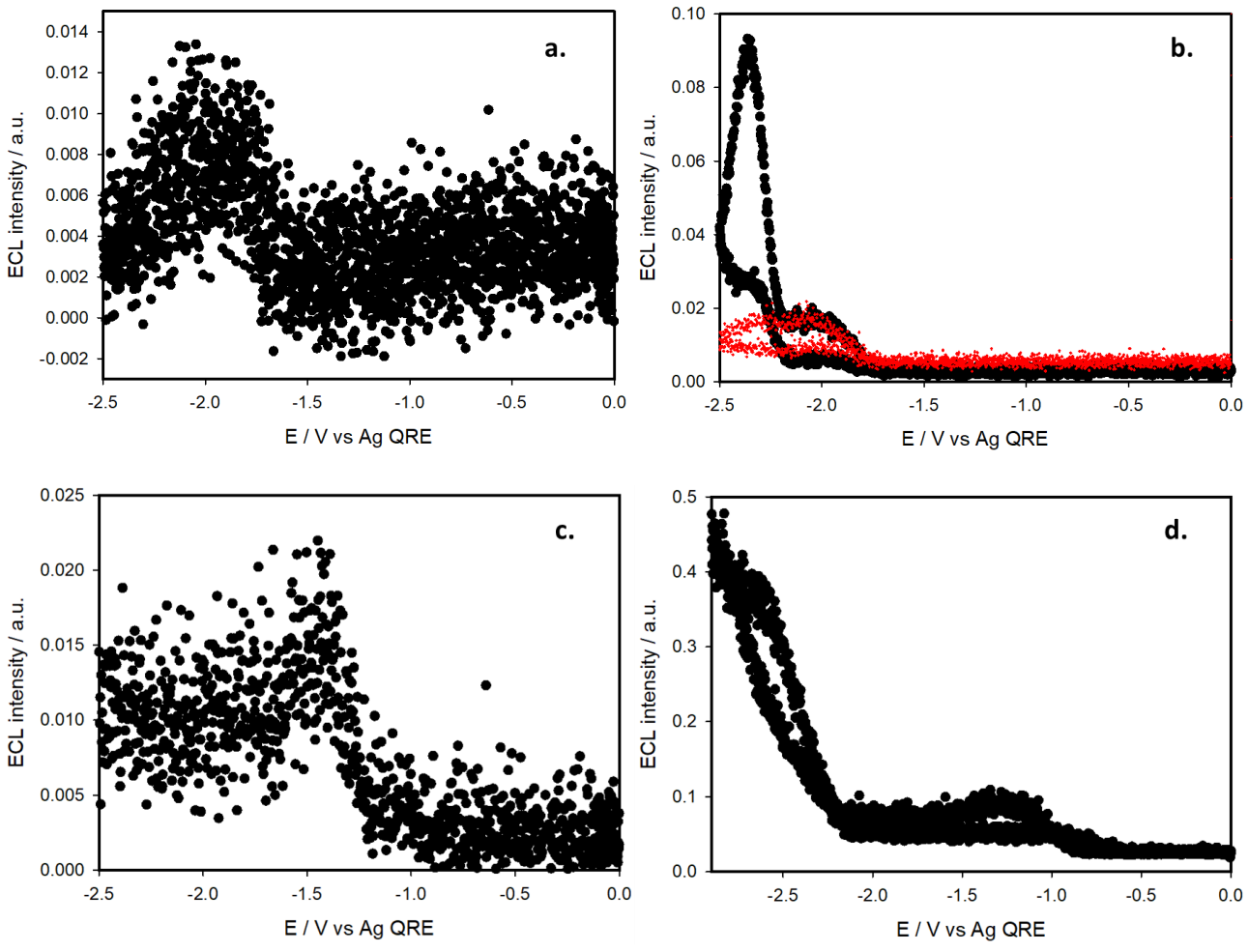

Figure 3. *ECL intensity of (a)* ***$Si_{4\text{-}nm}$-DDE****, (b)* ***$Si_{4\ nm}$-DPA****, (c)* ***$Si_{3\ nm}$-DDE****, and (d)* ***$Si_{3\ nm}$-DPA*** *in THF with BPO as coreactant (first cycle). Scan rate: 0.1 V/s. Panel b reports also the ECL intensity registered with a 550-nm cutoff filter (red dots).*

For 4-nm sized SiNCs (Figure 3a and b), electrochemiluminescence is observed at -2.0 V. For the **$Si_{4\ nm}$-DPA** sample (Figure 3b), a further ECL signal happens with maximum at -2.4 V. These two signals are attributed to SiNC and DPA electrogenerated emission, respectively. Indeed, upon registering ECL with a 550-nm cutoff filter, which eliminates the DPA emission, only the ECL signal at -2.0 V was observed (red dotted line in Figure 3b) as occurs for **$Si_{4\text{-}nm}$-DDE** (Figure 3a). Performing the same measurements on 3-nm sized nanoparticles (Figure 3c and d for **$Si_{3\ nm}$-DDE** and **$Si_{3\ nm}$-DPA**, respectively), the ECL behavior is similar to that observed for 4-nm nanoparticles apart from the fact that the emission associated to the silicon nanoparticle occurs at a lower potential (with a maximum comprised between -1.2 and -1.4 V). This behavior has been attributed to the different dimension of the nanoparticles.

Under these experimental conditions, SiNCs are stable since repeated cycles of CV and ECLs are reproducible. Chronoamperometry and the trend of the ECL signal over cycles can be found in the Supporting Information (Figure S6). It is worth noting that, for the samples functionalized with diphenylanthracene the emission of silicon is far less intense than DPA's one. This is probably due to the high number of DPA units per SiNC, which enhances the probability for the coreactants to encounter the organic fluorophore, and the steric hindrance of DPA which does not facilitate the diffusion of the coreactants towards the silicon surface. On the other hand, the emission of the silicon is enhanced compared to the dodecyl-passivated samples. A possible explanation is the different passivating molecules: 1-dodecene or chloro(dimethyl)vinylsilane for the first step of passivation with diphenylanthracene. The capping with the chlorosilane can result in a lower surface coverage compared to the alkyl chain, resulting in a better accessibility for the BPO coreactant in the diphenylanthracene containing sample.

In order to understand if silicon ECL is influenced by DPA, as it occurs for photoluminescence, ECL spectra were performed at different potentials (-2.0 V, -2.4 V and -2.5 V vs Ag QRE for **$Si_{4\ nm}$-DPA**, -2.0 and -2.7 V for **$Si_{3\ nm}$-DPA**). The emissions are collected in Figure 4.

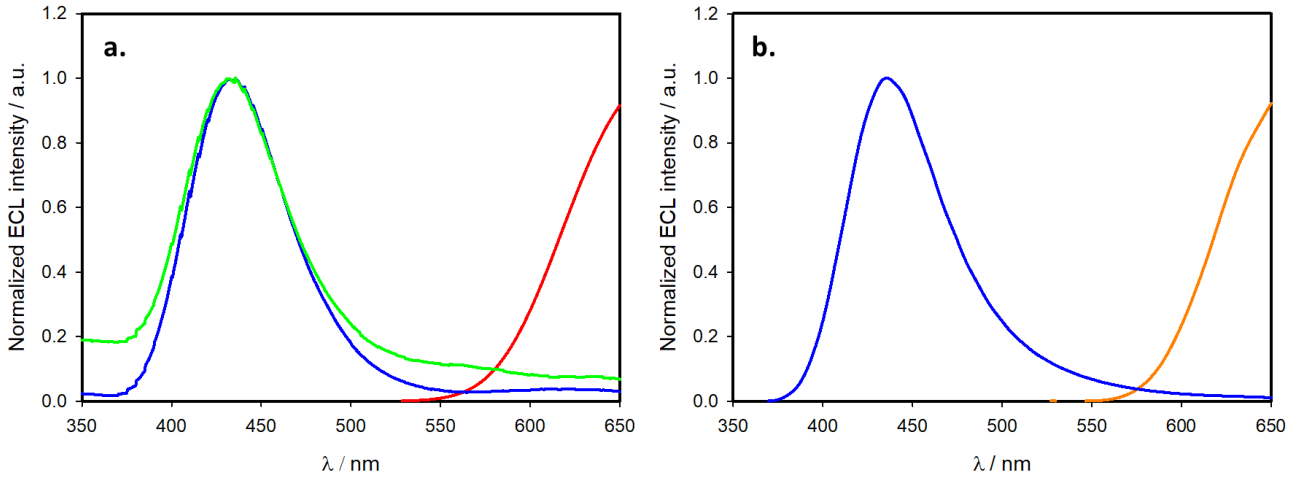

***Figure 4**. ECL spectra of (a) **$Si_{4\ nm}$-DPA** sample in THF with BPO as coreactant recorded at -2.0 V (red line), -2.4 V (blue line) and -2.5 V (green line) vs Ag QRE, (b) **$Si_{3\ nm}$-DPA** at -2.0 V (orange line) and -2.7 V (blue line).*

For the spectra recorded at -2.0 V, a single emission band is visible and it is associated to the silicon nanoparticle luminescence (red line in Figure 4a and orange line in Figure 4b). Unfortunately, the emission maximum is outside the sensitivity range of the photomultiplier used for ECL experiments, so that a direct comparison with the photoluminescence spectrum reported in Figure 2 is not possible. The DPA emission is not visible, confirming that at the potential under consideration, the organic chromophore is not reduced. Only the SiNC is reduced, the benzoyloxy radical reaches the quantum dot and the exciton is formed (Figure 5a). It is interesting however that the ECL spectrum of SiNCs (Figure 4) is reminiscent of their PL spectrum (Figure 2), even if only the high energy part can be observed in the ECL experiment for the different detector sensitivity. On the other hand, Bard[22] reported a strongly red-shifted ECL spectrum for SiNCs compared to their PL spectrum: this shift was attributed to different emissive states, in particular from the surface, where the energy gap was smaller.

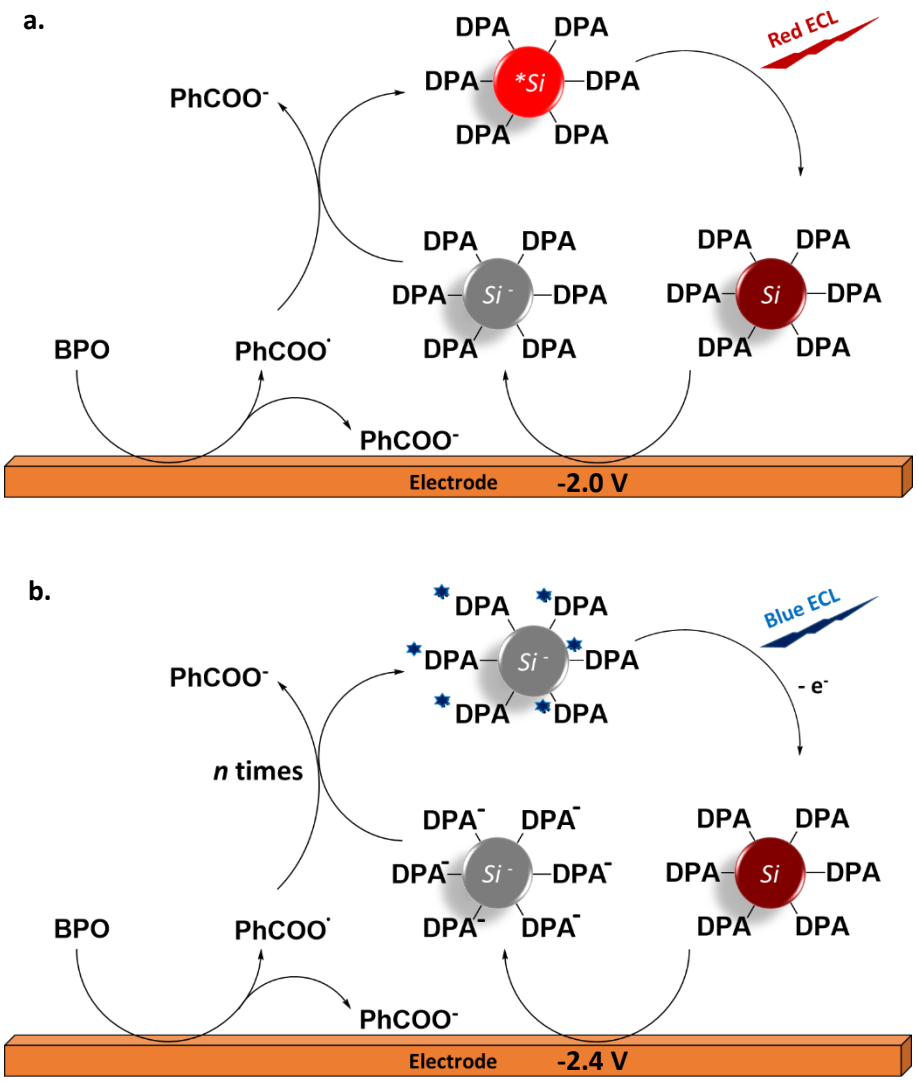

Figure 5. *Mechanism of electrochemiluminescence of diphenylanthracene-functionalized SiNCs at (a) -2.0 V and (b) -2.4 V with BPO as coreactant.*

Performing the measurements at lower potentials, the obtained ECL spectra look different (Figure 4, blue and green lines). In each case, only one significant emission is shown and it is attributed to the DPA (in accordance to the ECL spectrum of the ligand alone in Figure S4b).

Unlike photoexcitation, the experiment suggests that the antenna effect does not take place in consequence of the electrogenerated excitation of DPA. Our explanation is that at potentials more negative than -2.4 V vs Ag QRE, both the organic chromophore and the silicon nanocrystal are reduced. Benzoyloxy radical, before reaching the surface of silicon quantum dot, encounters the reduced DPA and generates its excited state. The energy transfer process to the SiNC does not occur,

likely made unfavorable by the presence of extra electrons in the conduction band of silicon, and the emission of DPA can take place without being affected (Figure 5b).

CONCLUSIONS

Concluding, we have proven that silicon nanocrystals functionalized with chromophores can display a dual-potential ECL, due to the emissions from the organic shell and the silicon nanocrystal, which are, unlike photoluminescence, independent from each other. Contrary to the existing dual-potential systems based on quantum dots, the potential at which the different ECLs occur has the same sign (in the presented case, negative potentials). This is useful if the electrochemical stability of the solvent does not allow to span a wide range of potentials.

Although the direct analytical application of this family of SiNCs is still under investigation in our laboratories we believe that the use of cheap and biocompatible SiNCs, in which the position of the valence and the conduction bands can be varied with the dimensions,[49] the possibility to modify them with different functional groups (for improve the water solubility) and with a high variety of luminophores (i.e. tunable ECL emission) can improve the current biosensing techniques.

ASSOCIATED CONTENT

Supporting information: ^{1}H-NMR of Si-DPA, correlation between size and emissive properties, calculation of the number of DPA per nanocrystal, evaluation of the enhancement of the brightness, measurements in DCM with TrPA, measurements on DPA, CVs of 3-nm sized Si-DDE and Si-DPA, stability of ECL signal and additional figures (PDF).

AUTHOR INFORMATION

Corresponding Authors

*Francesco Paolucci – Phone: +39 051 20 9 9460; Email: francesco.paolucci@unibo.it

*Paola Ceroni – Phone: +39 051 20 9 9535; Email: paola.ceroni@unibo.it

Notes

The authors declare no competing financial interest.

ACKNOWLEDGMENT

The University of Bologna is gratefully acknowledged for financial support.

REFERENCES

1 A. J. Bard, *Electrogenerated chemiluminescence*, Marcel Dekker: New York, 2004.

2 N. Sojic, *Analytical Electrogenerated Chemiluminescence: From Fundamentals to Bioassays. Detection Science.*, Royal Society of Chemistry (RSC) Publishing, 2020.

3 J. Forster, P. Bertoncello and E. Keyes, Electrogenerated Chemiluminescence, *Annu. Rev. Anal. Chem.*, 2009, **2**, 359–85.

4 W. Miao, Electrogenerated Chemiluminescence and Its Biorelated Applications, *Chem. Rev.*, 2008, **108**, 2506–2553.

5 Z. Liu, W. Qi and G. Xu, Recent advances in electrochemiluminescence, *Chem Soc Rev*, 2015, **44**, 3117–3142.

6 A. Fiorani, J. P. Merino, A. Zanut, A. Criado, G. Valenti, M. Prato and F. Paolucci, Electrochemistry Advanced carbon nanomaterials for electrochemiluminescent biosensor applications, *Curr. Opin. Electrochem.*, 2019, **16**, 66–74.

7 P. Bertoncello and P. Ugo, Recent Advances in Electrochemiluminescence with Quantum Dots and Arrays of Nanoelectrodes, *ChemElectroChem*, 2017, **4**, 1663–1676.

8 G. Valenti, E. Rampazzo, S. Kesarkar, D. Genovese, A. Fiorani, A. Zanut, F. Palomba, M. Marcaccio, F. Paolucci and L. Prodi, Electrogenerated chemiluminescence from metal complexes-based nanoparticles for highly sensitive sensors applications, *Coord. Chem. Rev.*, 2018, **367**, 65–81.

9 Y. Shan, J. Xu and H. Chen, Enhanced electrochemiluminescence quenching of CdS:Mn nanocrystals by CdTe QDs-doped silica nanoparticles for ultrasensitive detection of thrombin, *Nanoscale*, 2011, **3**, 2916–2923.

10 M. Farzin and H. Abdoos, A critical review on quantum dots: From synthesis toward applications in electrochemical biosensors for determination of disease-related biomolecules, *Talanta*, 2021, **224**, 121828.

11 S. Carrara, F. Arcudi, M. Prato and L. De Cola, Amine-Rich Nitrogen-Doped Carbon Nanodots as a Platform for Self-Enhancing Electrochemiluminescence, *Angew. Chem. Int. Ed.*, 2017, **56**, 4757–4761.

12 Y. Chen, Y. Cao, C. Ma and J. Zhu, Carbon-based dots for electrochemiluminescence sensing, *Mater. Chem. Front.*, 2020, **4**, 369–385.

13 F. Pinaud, L. Russo, S. Pinet, I. Gosse, V. Ravaine and N. Sojic, Enhanced electrogenerated chemiluminescence in thermoresponsive microgels, *J. Am. Chem. Soc.*, 2013, **135**, 5517–5520.

14 S. Kesarkar, S. Valente, A. Zanut, F. Palomba, A. Fiorani, M. Marcaccio, E. Rampazzo, G. Valenti, F. Paolucci and L. Prodi, Neutral Dye-Doped Silica Nanoparticles for Electrogenerated Chemiluminescence Signal Amplification, *J. Phys. Chem. C*, 2019, **123**, 5686–5691.

15 L. Zhang and S. Dong, Electrogenerated Chemiluminescence Sensors Using $[Ru(bpy)_3]^{2+}$ Doped in Silica Nanoparticles, *Anal. Chem.*, 2006, **78**, 5119–5123.

16 Z. Cao, Y. Shu, H. Qin, B. Su and X. Peng, Quantum Dots with Highly Efficient, Stable, and Multicolor Electrochemiluminescence, *ACS Cent. Sci.*, 2020, **6**, 1129–1137.

17 X. Feng, N. Gan, H. Zhang, Q. Yan, T. Li, Y. Cao, F. Hu, H. Yu and Q. Jiang, A novel "dual-potential" electrochemiluminescence aptasensor array using CdS quantum dots and luminol-gold nanoparticles as labels for simultaneous detection of malachite green and

chloramphenicol, *Biosens. Bioelectron.*, 2015, **74**, 587–593.

18 H. Zhang, M. Wu, J. Xu and H. Chen, Signal-On Dual-Potential Electrochemiluminescence Based on Luminol − Gold Bifunctional Nanoparticles for Telomerase Detection, *Anal. Chem.*, 2014, **86**, 3834–3840.

19 P. Wu, X. Hou, J. Xu and H. Chen, Ratiometric fluorescence, electrochemilumine- scence, and photoelectrochemical chemo/ biosensing based on semiconductor quantum dots, *Nanoscale*, 2016, **8**, 8427–8442.

20 X. Fu, X. Tan, R. Yuan and S. Chen, A dual-potential electrochemiluminescence ratiometric sensor for sensitive detection of dopamine based on graphene-CdTe quantum dots and self-enhanced Ru(II) complex, *Biosens. Bioelectron.*, 2017, **90**, 61–68.

21 R. Mazzaro, F. Romano and P. Ceroni, Long-lived luminescence of silicon nanocrystals: from principles to applications, *Phys. Chem. Chem. Phys.*, 2017, **19**, 26507–26526.

22 Z. Ding, B. M. Quinn, S. K. Haram, L. E. Pell, B. A. Korgel and A. J. Bard, Electrochemistry and Electrogenerated Chemiluminescence from Silicon Nanocrystal Quantum Dots, *Science*, 2002, **296**, 1293–1298.

23 Y. Dong, J. Wang, Y. Peng and J. Zhu, Electrogenerated chemiluminescence of Si quantum dots in neutral aqueous solution and its biosensing application, *Biosens. Bioelectron.*, 2017, **89**, 1053–1058.

24 Y. Dong, J. Wang, Y. Peng and J. Zhu, A novel aptasensor for lysozyme based on electrogenerated chemiluminescence resonance energy transfer between luminol and silicon quantum dots, *Biosens. Bioelectron.*, 2017, **94**, 530–535.

25 J. L. Z. Ddungu, S. Silvestrini, A. Tassoni and L. De Cola, Shedding light on the aqueous synthesis of silicon nanoparticles by reduction of silanes with citrates, *Faraday Discuss.*, 2020, **222**, 350–361.

26 B. V. Oliinyk, D. Korytko, V. Lysenko and S. Alekseev, Are Fluorescent Silicon Nanoparticles Formed in a One-Pot Aqueous Synthesis?, *Chem Mater*, 2019, **31**, 7167–7172.

27 Y. Mo, F. Li, B. Zheng, S. Yang, H. Yuan and Y. Guo, Enhancement of Electrochemiluminescence of Porous Silicon with Tri-n-propylamine as Co-reactant, *Electroanalysis*, 2012, **24**, 1887–1894.

28 W. H. Green, E. J. Lee, J. M. Lauerhaas, T. W. Bitner and M. J. Sailor, Electrochemiluminescence from porous silicon in formic acid liquid-junction cells, *Appl. Phys. Lett.*, 1995, **67**, 1468–1470.

29 J. Tan, L. Xu, T. Li, B. Su and J. Wu, Image-Contrast Technology Based on the Electrochemiluminescence of Porous Silicon and Its Application in Fingerprint Visualization, *Angew. Chem. Int. Ed.*, 2014, **53**, 9822–9826.

30 H. C. Choi and J. M. Buriak, Effects of Organic Monolayer Formation on Electrochemiluminescence Behavior of Porous Silicon, *Chem. Mater.*, 2000, **12**, 2151–2156.

31 Y. Cui, J. Jin, X. Chen and J. Wu, Two-Dimensional Electrochemiluminescence on Porous Silicon Platform for Explosive Detection and Discrimination, *ACS Sens.*, 2018, **3**, 1439–1444.

32 L. T. Canham, Silicon quantum wire array fabrication by electrochemical and chemical dissolution of wafers, *Appl. Phys. Lett.*, 1990, **57**, 1046–1048.

33 M. Locritani, Y. Yu, G. Bergamini, M. Baroncini, J. K. Molloy, B. A. Korgel and P. Ceroni, Silicon nanocrystals functionalized with pyrene units: Efficient light-harvesting antennae with bright near-infrared emission, *J. Phys. Chem. Lett.*, 2014, **5**, 3325–3329.

34 L. Ravotto, Q. Chen, Y. Ma, S. A. Vinogradov, M. Locritani, G. Bergamini, F. Negri, Y. Yu, B. A. Korgel and P. Ceroni, Bright Long-Lived Luminescence of Silicon Nanocrystals Sensitized by Two-Photon Absorbing Antenna, *Chem*, 2017, **2**, 550–560.

35 A. Fermi, M. Locritani, D. Carlo, M. Pizzotti, S. Caramori, Y. Yu, B. A. Korgel and P. Ceroni, Light-harvesting antennae based on photoactive silicon nanocrystals functionalized with porphyrin chromophores, *Faraday Discuss.*, 2015, **185**, 481–495.

36 R. Mazzaro, A. Gradone, S. Angeloni, G. Morselli, P. G. Cozzi, F. Romano, A. Vomiero and P. Ceroni, Hybrid Silicon Nanocrystals for Color-Neutral and Transparent Luminescent Solar Concentrators, *ACS Photonics*, 2019, **6**, 2303–2311.

37 G. Morselli, F. Romano and P. Ceroni, Amine functionalised silicon nanocrystals with bright red and long-lived emission, *Faraday Discuss.*, 2020, **222**, 108–121.

38 H. Chen, W. Li, Q. Wang, X. Jin, Z. Nie and S. Yao, Nitrogen doped graphene quantum dots based single-luminophor generated dual-potential electrochemiluminescence system for ratiometric sensing of Co^{2+} ion, *Electrochim. Acta*, 2016, **214**, 94–102.

39 H. Zhao, R. Liang, J. Wang and J. Qiu, A dual-potential electrochemiluminescence dots and luminol for highly sensitive detection of protein kinase activity, *Chem. Commun.*, 2015, **51**, 12669–12672.

40 Y. Liu, Y. Sun and M. Yang, A double-potential ratiometric electrochemiluminescence platform based on g-C_3N_4 nanosheets (g-C_3N_4 NSs) and graphene quantum dots for Cu^{2+} detection, *Anal. Methods*, DOI:10.1039/d0ay02233k.

41 X. Wang, H. Liu, H. Qi, Q. Gao and C. Zhang, Highly efficient electrochemiluminescence of ruthenium complex-functionalized CdS quantum dots and their analytical application, *J. Mater. Chem. B*, 2020, **8**, 3598–3605.

42 M. R. . Hessel, C. M.; Reid, D.; Panthani, M. G.; Rasch and B. A. Goodfellow, B. W.; Wei, J.; Fujii, H.; Akhavan, V.; Korgel, Synthesis of Ligand-Stabilized Silicon Nanocrystals with Size-Dependent Photoluminescence Spanning Visible to Near-Infrared Wavelengths, *Chem. Mater*, 2012, **24**, 393−401.

43 R. J. Clark, M. Aghajamali, C. M. Gonzalez, L. Hadidi, M. A. Islam, M. Javadi, H. Mobarok, T. K. Purkait, C. J. T. Robidillo, R. Sinelnikov, A. N. Thiessen, J. Washington, H. Yu and J. G. C. Veinot, From Hydrogen Silsesquioxane to Functionalized Silicon Nanocrystals, *Chem Mater*, 2017, **29**, 80–89.

44 M. Montalti, A. Credi, L. Prodi and M. T. Gandolfi, *Handbook of photochemistry*, Taylor & Francis, 3 ed., 2006.

45 V. Balzani, P. Ceroni and A. Juris, *Photochemistry and Photophysics - Concepts, Research, Applications*, Wiley-VCH, 1 ed., 2015.

46 G. A. Crosby and J. N. Demas, Measurement of photoluminescence quantum yields. Review, *J. Phys. Chem.*, 1971, **75**, 991–1024.

47 Y. Yu, G. Fan, A. Fermi, R. Mazzaro, V. Morandi, P. Ceroni, D.M. Smilgies and B. A. Korgel, Size-Dependent Photoluminescence Efficiency of Silicon Nanocrystal Quantum Dots, *J. Phys. Chem. C*, 2017, **121**, 23240–23248.

48 C. M. Hessel, E. J. Henderson and J. G. C. Veinot, Hydrogen Silsesquioxane: A Molecular Precursor for Nanocrystalline Si−SiO_2 Composites and Freestanding Hydride-Surface-Terminated Silicon Nanoparticles, *Chem. Mater.*, 2006, **18**, 6139–6146.

49 A. Arrigo, R. Mazzaro, F. Romano, G. Bergamini and P. Ceroni, Photoinduced electron-transfer quenching of luminescent silicon nanocrystals as a way to estimate the position of the conduction and valence bands by Marcus theory, *Chem. Mater.*, 2016, **28**, 6664–6671.

50 I. M. D. Hohlein, J. Kehrle, J. G. C. Veinot and B. Rieger, Photoluminescent silicon nanocrystals with chlorosilane surfaces – synthesis and reactivity, *Nanoscale*, 2015, **7**, 914–918.

51 G. Valenti, C. Bruno, S. Rapino, A. Fiorani, E. A. Jackson, L. T. Scott, F. Paolucci and M. Marcaccio, Intense and Tunable Electrochemiluminescence of Corannulene, *J. Phys. Chem.*

C, 2010, **114**, 19467–19472.

Graphical TOC Entry